SUPPLEMENTARY MATERIALS: ACTIVE FLUX METHODS FOR HYPERBOLIC CONSERVATION LAWS – FLUX VECTOR SPLITTING AND BOUND-PRESERVATION*

JUNMING DUAN†, WASILIJ BARSUKOW‡, AND CHRISTIAN KLINGENBERG§

SM1. 2D flux vector splitting.

SM1.1. Local Lax-Friedrichs flux vector splitting. This flux vector splitting can be written as

$$\boldsymbol{F}_\ell^\pm = \frac{1}{2}(\boldsymbol{F}_\ell(\boldsymbol{U}) \pm \alpha_\ell \boldsymbol{U}),$$

where α_ℓ is determined by

$$(\alpha_1)_{i+\frac{1}{2},q} = \max_s \left\{|\varrho_1(\boldsymbol{U}_{s,q})|\right\},\ s \in \left\{i-\frac{1}{2}, i, i+\frac{1}{2}, i+1, i+\frac{3}{2}\right\}, q = j, j+\frac{1}{2},$$

$$(\alpha_2)_{q,j+\frac{1}{2}} = \max_s \left\{|\varrho_2(\boldsymbol{U}_{q,s})|\right\},\ s \in \left\{j-\frac{1}{2}, j, j+\frac{1}{2}, j+1, j+\frac{3}{2}\right\}, q = i, i+\frac{1}{2},$$

and ϱ_ℓ is the spectral radius of the Jacobian matrix $\partial \boldsymbol{F}_\ell / \partial \boldsymbol{U}$.

SM1.2. Upwind flux vector splitting. The flux can also be split based on each characteristic field as follows

$$\boldsymbol{F}_\ell^\pm = \frac{1}{2}(\boldsymbol{F}_\ell(\boldsymbol{U}) \pm |\boldsymbol{J}_\ell| \boldsymbol{U}), \quad |\boldsymbol{J}_\ell| = \boldsymbol{R}_\ell(\boldsymbol{\Lambda}_\ell^+ - \boldsymbol{\Lambda}_\ell^-)\boldsymbol{R}_\ell^{-1}, \tag{SM1.1}$$

with $\boldsymbol{J}_\ell = \partial \boldsymbol{F}_\ell / \partial \boldsymbol{U} = \boldsymbol{R}_\ell \boldsymbol{\Lambda}_\ell \boldsymbol{R}_\ell^{-1}$ the eigen-decomposition of the Jacobian matrix.

For the Euler equations, the explicit expressions in the x-direction are

$$\boldsymbol{F}_1^\pm = \begin{bmatrix} \frac{\rho}{2\gamma}\alpha^\pm \\ \frac{\rho}{2\gamma}\left(\alpha^\pm v_1 + a(\lambda_2^\pm - \lambda_3^\pm)\right) \\ \frac{\rho}{2\gamma}\alpha^\pm v_2 \\ \frac{\rho}{2\gamma}\left(\frac{1}{2}\alpha^\pm \left\|\boldsymbol{v}\right\|_2^2 + a v_1(\lambda_2^\pm - \lambda_3^\pm) + \frac{a^2}{\gamma-1}(\lambda_2^\pm + \lambda_3^\pm)\right) \end{bmatrix},$$

where $\lambda_1 = v_\ell,\ \lambda_2 = v_\ell + a,\ \lambda_3 = v_\ell - a,\ \alpha^\pm = 2(\gamma-1)\lambda_1^\pm + \lambda_2^\pm + \lambda_3^\pm$, and $a = \sqrt{\gamma p/\rho}$ is the sound speed. The expressions in the y-direction can be obtained using the rotational invariance.

---

*Submitted to the editors DATE.

Funding: JD was supported by an Alexander von Humboldt Foundation Research Fellowship CHN-1234352-HFST-P. CK and WB acknowledge funding by the Deutsche Forschungsgemeinschaft (DFG, German Research Foundation) within *SPP 2410 Hyperbolic Balance Laws in Fluid Mechanics: Complexity, Scales, Randomness (CoScaRa)*, project number 525941602.

†Corresponding author. Institute of Mathematics, University of Würzburg, Emil-Fischer-Straße 40, 97074 Würzburg, Germany (junming.duan@uni-wuerzburg.de).

‡Institut de Mathématiques de Bordeaux (IMB), CNRS UMR 5251, University of Bordeaux, 33405 Talence, France (wasilij.barsukow@math.u-bordeaux.fr).

§Institute of Mathematics, University of Würzburg, Emil-Fischer-Straße 40, 97074 Würzburg, Germany (christian.klingenberg@uni-wuerzburg.de).

SM1.3. Van Leer-Hänel flux vector splitting for the Euler equations. For the x-direction, the flux is split according to the Mach number $M = v_1/a$ as

$$\boldsymbol{F}_1 = \begin{bmatrix} \rho a M \\ \rho a^2 (M^2 + \frac{1}{\gamma}) \\ \rho a M v_2 \\ \rho a^3 M (\frac{1}{2} M^2 + \frac{1}{\gamma - 1}) + \frac{\rho a M v_2^2}{2} \end{bmatrix} = \boldsymbol{F}_1^+ + \boldsymbol{F}_1^-, \;\; \boldsymbol{F}_1^\pm = \begin{bmatrix} \pm \frac{1}{4} \rho a (M \pm 1)^2 \\ \pm \frac{1}{4} \rho a (M \pm 1)^2 v_1 + p^\pm \\ \pm \frac{1}{4} \rho a (M \pm 1)^2 v_2 \\ \pm \frac{1}{4} \rho a (M \pm 1)^2 H \end{bmatrix}$$

with the enthalpy $H = (E + p)/\rho$, and the pressure-splitting $p^\pm = \frac{1}{2}(1 \pm \gamma M) p$.

SM2. Bound-preserving property of intermediate states. Similar to the proofs in [SM18, SM19], the following lemmas hold.

LEMMA SM2.1. *For the scalar conservation laws* (3.2)*, the intermediate state* $\widetilde{u} = \frac{1}{2}(u_L + u_R) + \frac{1}{2\alpha}(f_\ell(u_L) - f_\ell(u_R))$ *stays in* $\mathcal{G}$ (4.1) *if* $\alpha \geqslant \max\{\varrho_\ell(u_L), \varrho_\ell(u_R)\}$.

Proof. The partial derivatives of the intermediate state satisfy

$$\frac{\partial \widetilde{u}(u_L, u_R)}{\partial u_L} = \frac{1}{2}\left(1 + \frac{f_\ell'(u_L)}{\alpha}\right) \geqslant 0, \quad \frac{\partial \widetilde{u}(u_L, u_R)}{\partial u_R} = \frac{1}{2}\left(1 - \frac{f_\ell'(u_R)}{\alpha}\right) \geqslant 0.$$

As $\widetilde{u}(m_0, m_0) = m_0$, $\widetilde{u}(M_0, M_0) = M_0$, it holds $m_0 \leqslant \widetilde{u} \leqslant M_0$. ∎

LEMMA SM2.2. *For the Euler equations, the intermediate state* $\widetilde{\boldsymbol{U}} = \frac{1}{2}(\boldsymbol{U}_L + \boldsymbol{U}_R) + \frac{1}{2\alpha}(\boldsymbol{F}_\ell(\boldsymbol{U}_L) - \boldsymbol{F}_\ell(\boldsymbol{U}_R))$ *stays in* $\mathcal{G}$ (4.2) *if* $\alpha \geqslant \max\{\varrho_\ell(\boldsymbol{U}_L), \varrho_\ell(\boldsymbol{U}_R)\}$.

Proof. For the Euler equations, as the intermediate state is a convex combination of $\boldsymbol{U}_L - \frac{1}{\alpha}\boldsymbol{F}_\ell(\boldsymbol{U}_L)$ and $\boldsymbol{U}_R + \frac{1}{\alpha}\boldsymbol{F}_\ell(\boldsymbol{U}_R)$, we only need to show that the $\boldsymbol{U} \pm \frac{1}{\alpha}\boldsymbol{F}_\ell(\boldsymbol{U})$ belongs to $\mathcal{G}$. The density component $(\rho \pm (\rho v_\ell)/\alpha)$ is positive since $\alpha > |v_\ell|$. The recovered internal energy is

$$\begin{aligned} \rho e\left(\boldsymbol{U} \pm \frac{1}{\alpha}\boldsymbol{F}_\ell(\boldsymbol{U})\right) &= E\left(\boldsymbol{U} \pm \frac{1}{\alpha}\boldsymbol{F}_\ell(\boldsymbol{U})\right) - \frac{\left\|\rho \boldsymbol{v}\left(\boldsymbol{U} \pm \frac{1}{\alpha}\boldsymbol{F}_\ell(\boldsymbol{U})\right)\right\|_2^2}{2\rho\left(\boldsymbol{U} \pm \frac{1}{\alpha}\boldsymbol{F}_\ell(\boldsymbol{U})\right)} \\ &= \left(1 - \frac{p^2}{2(\alpha \pm v_\ell)^2 \rho^2 e}\right)\left(1 \pm \frac{v_\ell}{\alpha}\right)\rho e, \end{aligned}$$

so that one has $\rho e\left(\boldsymbol{U} \pm \frac{1}{\alpha}\boldsymbol{F}_\ell(\boldsymbol{U})\right) > 0 \iff \frac{p^2}{2\rho^2 e} < (\alpha \pm v_\ell)^2 \iff \frac{\gamma - 1}{2\gamma} a^2 < (\alpha \pm v_\ell)^2$ for the perfect gas EOS, which holds as $\alpha \geqslant |v_\ell| + a$. ∎

SM3. 1D bound-preserving active flux methods. For the scalar conservation law (2.2), its solutions satisfy a strict maximum principle (MP) [SM5], i.e.,

(SM3.1) $$\mathcal{G} = \{u \mid m_0 \leqslant u \leqslant M_0\}, \quad m_0 = \min_x u_0(x), \; M_0 = \max_x u_0(x).$$

For the compressible Euler equations, the admissible state set is

(SM3.2) $$\mathcal{G} = \left\{\boldsymbol{U} = (\rho, \rho v, E) \;\middle|\; \rho > 0, \; p = (\gamma - 1)\left(E - (\rho v)^2/(2\rho)\right) > 0\right\}.$$

which is convex, see e.g. [SM21].

SM3.1. Convex limiting for the cell average. This section presents a convex limiting approach to achieve the BP property of the cell average update. The low-order scheme is chosen as the first-order LLF scheme

$$\overline{\boldsymbol{U}}_i^{\mathtt{L}} = \overline{\boldsymbol{U}}_i^n - \mu_i \left(\widehat{\boldsymbol{F}}_{i+\frac{1}{2}}^{\mathtt{L}} - \widehat{\boldsymbol{F}}_{i-\frac{1}{2}}^{\mathtt{L}} \right), \quad \mu_i = \Delta t^n / \Delta x_i,$$
$$\widehat{\boldsymbol{F}}_{i+\frac{1}{2}}^{\mathtt{L}} = \boldsymbol{F}^{\mathrm{LLF}}(\overline{\boldsymbol{U}}_i^n, \overline{\boldsymbol{U}}_{i+1}^n) = \frac{1}{2}\left(\boldsymbol{F}(\overline{\boldsymbol{U}}_i^n) + \boldsymbol{F}(\overline{\boldsymbol{U}}_{i+1}^n) \right) - \frac{\alpha_{i+\frac{1}{2}}}{2} \left(\overline{\boldsymbol{U}}_{i+1}^n - \overline{\boldsymbol{U}}_i^n \right),$$
$$\alpha_{i+\frac{1}{2}} = \max\{ \varrho(\overline{\boldsymbol{U}}_i^n),\ \varrho_\ell(\overline{\boldsymbol{U}}_{i+1}^n) \},$$

where ϱ is the spectral radius of $\partial \boldsymbol{F}/\partial \boldsymbol{U}$. Note that here $\alpha_{i+\frac{1}{2}}$ is not the same as the one in the LLF FVS (2.12). Following [SM8], the first-order LLF scheme can be rewritten as

$$\overline{\boldsymbol{U}}_i^{\mathtt{L}} = \left[1 - \mu_i \left(\alpha_{i-\frac{1}{2}} + \alpha_{i+\frac{1}{2}} \right) \right] \overline{\boldsymbol{U}}_i^n + \mu_i \alpha_{i-\frac{1}{2}} \widetilde{\boldsymbol{U}}_{i-\frac{1}{2}} + \mu_i \alpha_{i+\frac{1}{2}} \widetilde{\boldsymbol{U}}_{i+\frac{1}{2}}, \tag{SM3.3}$$

with the first-order LLF intermediate states defined as

$$\widetilde{\boldsymbol{U}}_{i\pm\frac{1}{2}} \coloneqq \frac{1}{2}\left(\overline{\boldsymbol{U}}_i^n + \overline{\boldsymbol{U}}_{i\pm1}^n \right) \pm \frac{1}{2\alpha_{i\pm\frac{1}{2}}} \left[\boldsymbol{F}(\overline{\boldsymbol{U}}_i^n) - \boldsymbol{F}(\overline{\boldsymbol{U}}_{i\pm1}^n) \right]. \tag{SM3.4}$$

The proofs of $\widetilde{\boldsymbol{U}}_{i\pm\frac{1}{2}} \in \mathcal{G}$ are similar to Section SM2, for the scalar case and Euler equations.

Lemma SM3.1. If the time step size Δt^n satisfies

$$\Delta t^n \leqslant \frac{\Delta x_i}{\alpha_{i-\frac{1}{2}} + \alpha_{i+\frac{1}{2}}}, \tag{SM3.5}$$

then (SM3.3) is a convex combination, and the first-order LLF scheme is BP.

The proof (see e.g. [SM8, SM15]) relies on $\overline{\boldsymbol{U}}_i^n, \widetilde{\boldsymbol{U}}_{i\pm\frac{1}{2}} \in \mathcal{G}$ and the convexity of $\mathcal{G}$.

Upon defining the anti-diffusive flux $\Delta\widehat{\boldsymbol{F}}_{i\pm\frac{1}{2}} \coloneqq \widehat{\boldsymbol{F}}_{i\pm\frac{1}{2}}^{\mathtt{H}} - \widehat{\boldsymbol{F}}_{i\pm\frac{1}{2}}^{\mathtt{L}}$ with $\widehat{\boldsymbol{F}}_{i\pm\frac{1}{2}}^{\mathtt{H}} \coloneqq \boldsymbol{F}(\boldsymbol{U}_{i\pm\frac{1}{2}})$, a forward-Euler step applied to the semi-discrete high-order scheme for the cell average (2.4) can be written as

$$\begin{aligned} \overline{\boldsymbol{U}}_i^{\mathtt{H}} &= \overline{\boldsymbol{U}}_i^n - \mu_i (\widehat{\boldsymbol{F}}_{i+\frac{1}{2}}^{\mathtt{H}} - \widehat{\boldsymbol{F}}_{i-\frac{1}{2}}^{\mathtt{H}}) = \overline{\boldsymbol{U}}_i^n - \mu_i (\widehat{\boldsymbol{F}}_{i+\frac{1}{2}}^{\mathtt{L}} - \widehat{\boldsymbol{F}}_{i-\frac{1}{2}}^{\mathtt{L}}) - \mu_i (\Delta\widehat{\boldsymbol{F}}_{i+\frac{1}{2}} - \Delta\widehat{\boldsymbol{F}}_{i-\frac{1}{2}}) \\ &= \left[1 - \mu_i \left(\alpha_{i-\frac{1}{2}} + \alpha_{i+\frac{1}{2}} \right) \right] \overline{\boldsymbol{U}}_i^n + \mu_i \alpha_{i-\frac{1}{2}} \widetilde{\boldsymbol{U}}_{i-\frac{1}{2}}^{\mathtt{H},+} + \mu_i \alpha_{i+\frac{1}{2}} \widetilde{\boldsymbol{U}}_{i+\frac{1}{2}}^{\mathtt{H},-}, \end{aligned} \tag{SM3.6}$$
$$\widetilde{\boldsymbol{U}}_{i-\frac{1}{2}}^{\mathtt{H},+} \coloneqq \left(\widetilde{\boldsymbol{U}}_{i-\frac{1}{2}} + \frac{\Delta\widehat{\boldsymbol{F}}_{i-\frac{1}{2}}}{\alpha_{i-\frac{1}{2}}} \right), \quad \widetilde{\boldsymbol{U}}_{i+\frac{1}{2}}^{\mathtt{H},-} \coloneqq \left(\widetilde{\boldsymbol{U}}_{i+\frac{1}{2}} - \frac{\Delta\widehat{\boldsymbol{F}}_{i+\frac{1}{2}}}{\alpha_{i+\frac{1}{2}}} \right).$$

With the low-order scheme (SM3.3) and high-order scheme (SM3.6) having the same abstract form, one can blend them to define the limited scheme for the cell average as

$$\overline{\boldsymbol{U}}_i^{\mathtt{Lim}} = \left[1 - \mu_i \left(\alpha_{i-\frac{1}{2}} + \alpha_{i+\frac{1}{2}} \right) \right] \overline{\boldsymbol{U}}_i^n + \mu_i \alpha_{i-\frac{1}{2}} \widetilde{\boldsymbol{U}}_{i-\frac{1}{2}}^{\mathtt{Lim},+} + \mu_i \alpha_{i+\frac{1}{2}} \widetilde{\boldsymbol{U}}_{i+\frac{1}{2}}^{\mathtt{Lim},-}, \tag{SM3.7}$$

where the limited intermediate states are

$$\widetilde{\boldsymbol{U}}_{i\pm\frac{1}{2}}^{\mathtt{Lim},\mp} = \widetilde{\boldsymbol{U}}_{i\pm\frac{1}{2}} \mp \frac{\Delta\widehat{\boldsymbol{F}}_{i\pm\frac{1}{2}}^{\mathtt{Lim}}}{\alpha_{i\pm\frac{1}{2}}} \coloneqq \widetilde{\boldsymbol{U}}_{i\pm\frac{1}{2}} \mp \frac{\theta_{i\pm\frac{1}{2}} \Delta\widehat{\boldsymbol{F}}_{i\pm\frac{1}{2}}}{\alpha_{i\pm\frac{1}{2}}}, \tag{SM3.8}$$

and $\theta_{i\pm\frac{1}{2}} \in [0,1]$ are the blending coefficients. The limited scheme (SM3.7) reduces to the first-order LLF scheme if $\theta_{i\pm\frac{1}{2}} = 0$, and recovers the high-order AF scheme (2.4) when $\theta_{i\pm\frac{1}{2}} = 1$.

SM3.1.1. Application to scalar conservation laws. Similar to the 2D case, the convex limiting is applied to scalar conservation laws (2.2), such that the limited cell averages (SM3.7) satisfy the MP $u_i^{\min} \leqslant \bar{u}_i^{\mathtt{Lim}} \leqslant u_i^{\max}$, where $u_i^{\min} = \min \mathcal{N}$, $u_i^{\max} = \max \mathcal{N}$, and $\mathcal{N}$ will be defined later. The limited anti-diffusive flux is

$$\Delta \hat{f}^{\mathtt{Lim}}_{i+\frac{1}{2}} = \begin{cases} \min\left\{\Delta \hat{f}_{i+\frac{1}{2}},\ \alpha_{i+\frac{1}{2}}(\tilde{u}_{i+\frac{1}{2}} - u_i^{\min}),\ \alpha_{i+\frac{1}{2}}(u_{i+1}^{\max} - \tilde{u}_{i+\frac{1}{2}})\right\}, & \text{if } \Delta \hat{f}_{i+\frac{1}{2}} \geqslant 0, \\ \max\left\{\Delta \hat{f}_{i+\frac{1}{2}},\ \alpha_{i+\frac{1}{2}}(u_{i+1}^{\min} - \tilde{u}_{i+\frac{1}{2}}),\ \alpha_{i+\frac{1}{2}}(\tilde{u}_{i+\frac{1}{2}} - u_i^{\max})\right\}, & \text{otherwise.} \end{cases}$$

Finally, the limited numerical flux is

$$\hat{f}^{\mathtt{Lim}}_{i+\frac{1}{2}} = \hat{f}^{\mathtt{L}}_{i+\frac{1}{2}} + \Delta \hat{f}^{\mathtt{Lim}}_{i+\frac{1}{2}}. \tag{SM3.9}$$

If considering the global MP, $\mathcal{N} = \bigcup_i \{\bar{u}_i^n, u_{i+\frac{1}{2}}^n\}$. For the local MP, one can choose $\mathcal{N} = \min\left\{\bar{u}_i^n,\ \tilde{u}_{i-\frac{1}{2}},\ \tilde{u}_{i+\frac{1}{2}}, \bar{u}_{i-1}^n, \bar{u}_{i+1}^n\right\}$, which consists of the neighboring cell averages and intermediate states.

SM3.1.2. Application to the compressible Euler equations. This section aims at enforcing the positivity of density and pressure. To avoid the effect of the round-off error, we need to choose the desired lower bounds. Denote the lowest density and pressure in the domain by

$$\varepsilon^\rho := \min_i\{\overline{\boldsymbol{U}}_i^{n,\rho}, \boldsymbol{U}_{i+\frac{1}{2}}^{n,\rho}\},\ \varepsilon^p := \min_i\{p(\overline{\boldsymbol{U}}_i^n), p(\boldsymbol{U}_{i+\frac{1}{2}}^n)\}, \tag{SM3.10}$$

where $\boldsymbol{U}^{*,\rho}$ and $p(\boldsymbol{U}^*)$ denote the density component and pressure recovered from $\boldsymbol{U}^*$, respectively. The limiting (SM3.8) is feasible if the constraints are satisfied by the first-order LLF intermediate states (SM3.4), thus the lower bounds can be defined as

$$\varepsilon_i^\rho := \min\{10^{-13}, \varepsilon^\rho, \widetilde{\boldsymbol{U}}_{i-\frac{1}{2}}^\rho, \widetilde{\boldsymbol{U}}_{i+\frac{1}{2}}^\rho\},\ \varepsilon_i^p := \min\{10^{-13}, \varepsilon^p, p(\widetilde{\boldsymbol{U}}_{i-\frac{1}{2}}), p(\widetilde{\boldsymbol{U}}_{i+\frac{1}{2}})\}.$$

i) **Positivity of density.** The first step is to impose the density positivity $\widetilde{\boldsymbol{U}}_{i+\frac{1}{2}}^{\mathtt{Lim},\pm,\rho} \geqslant \bar{\varepsilon}_{i+\frac{1}{2}}^\rho := \min\{\varepsilon_i^\rho, \varepsilon_{i+1}^\rho\}$. Similarly to the derivation of the scalar case, the corresponding density component of the limited anti-diffusive flux is

$$\Delta \widehat{\boldsymbol{F}}^{\mathtt{Lim},*,\rho}_{i+\frac{1}{2}} = \begin{cases} \min\left\{\Delta \widehat{\boldsymbol{F}}^\rho_{i+\frac{1}{2}},\ \alpha_{i+\frac{1}{2}}\left(\widetilde{\boldsymbol{U}}^\rho_{i+\frac{1}{2}} - \bar{\varepsilon}^\rho_{i+\frac{1}{2}}\right)\right\}, & \text{if } \Delta \widehat{\boldsymbol{F}}^\rho_{i+\frac{1}{2}} \geqslant 0, \\ \max\left\{\Delta \widehat{\boldsymbol{F}}^\rho_{i+\frac{1}{2}},\ \alpha_{i+\frac{1}{2}}\left(\bar{\varepsilon}^\rho_{i+\frac{1}{2}} - \widetilde{\boldsymbol{U}}^\rho_{i+\frac{1}{2}}\right)\right\}, & \text{otherwise.} \end{cases}$$

Then the density component of the limited flux is $\widehat{\boldsymbol{F}}^{\mathtt{Lim},*,\rho}_{i+\frac{1}{2}} = \widehat{\boldsymbol{F}}^{\mathtt{L},\rho}_{i+\frac{1}{2}} + \Delta \widehat{\boldsymbol{F}}^{\mathtt{Lim},*,\rho}_{i+\frac{1}{2}}$, with the other components remaining the same as $\widehat{\boldsymbol{F}}^{\mathtt{H}}_{i+\frac{1}{2}}$.

ii) **Positivity of pressure.** The second step is to enforce pressure positivity $p(\widetilde{\boldsymbol{U}}^{\mathtt{Lim},\pm}_{i+\frac{1}{2}}) \geqslant \bar{\varepsilon}^p_{i+\frac{1}{2}} := \min\{\varepsilon_i^p, \varepsilon_{i+1}^p\}$. Since

$$\widetilde{\boldsymbol{U}}^{\mathtt{Lim},\pm}_{i+\frac{1}{2}} = \widetilde{\boldsymbol{U}}_{i+\frac{1}{2}} \pm \frac{\theta_{i+\frac{1}{2}} \Delta \widehat{\boldsymbol{F}}^{\mathtt{Lim},*}_{i+\frac{1}{2}}}{\alpha_{i+\frac{1}{2}}}, \quad \Delta \widehat{\boldsymbol{F}}^{\mathtt{Lim},*}_{i+\frac{1}{2}} = \widehat{\boldsymbol{F}}^{\mathtt{Lim},*}_{i+\frac{1}{2}} - \widehat{\boldsymbol{F}}^{\mathtt{L}}_{i+\frac{1}{2}},$$

the constraints lead to two inequalities

$$A_{i+\frac{1}{2}} \theta^2_{i+\frac{1}{2}} \pm B_{i+\frac{1}{2}} \theta_{i+\frac{1}{2}} \leqslant C_{i+\frac{1}{2}}, \tag{SM3.11}$$

with the coefficients

$$A_{i+\frac{1}{2}} = \frac{1}{2}\left(\Delta\widehat{\boldsymbol{F}}^{\texttt{Lim},*,\rho v}_{i+\frac{1}{2}}\right)^2 - \Delta\widehat{\boldsymbol{F}}^{\texttt{Lim},*,\rho}_{i+\frac{1}{2}}\Delta\widehat{\boldsymbol{F}}^{\texttt{Lim},*,E}_{i+\frac{1}{2}},$$

$$B_{i+\frac{1}{2}} = \alpha_{i+\frac{1}{2}}\left(\Delta\widehat{\boldsymbol{F}}^{\texttt{Lim},*,\rho}_{i+\frac{1}{2}}\widetilde{\boldsymbol{U}}^{E}_{i+\frac{1}{2}} + \widetilde{\boldsymbol{U}}^{\rho}_{i+\frac{1}{2}}\Delta\widehat{\boldsymbol{F}}^{\texttt{Lim},*,E}_{i+\frac{1}{2}} - \Delta\widehat{\boldsymbol{F}}^{\texttt{Lim},*,\rho v}_{i+\frac{1}{2}}\widetilde{\boldsymbol{U}}^{\rho v}_{i+\frac{1}{2}} - \tilde{\varepsilon}\Delta\widehat{\boldsymbol{F}}^{\texttt{Lim},*,\rho}_{i+\frac{1}{2}}\right),$$

$$C_{i+\frac{1}{2}} = \alpha^2_{i+\frac{1}{2}}\left(\widetilde{\boldsymbol{U}}^{\rho}_{i+\frac{1}{2}}\widetilde{\boldsymbol{U}}^{E}_{i+\frac{1}{2}} - \frac{1}{2}\left(\widetilde{\boldsymbol{U}}^{\rho v}_{i+\frac{1}{2}}\right)^2 - \tilde{\varepsilon}\widetilde{\boldsymbol{U}}^{\rho}_{i+\frac{1}{2}}\right), \quad \tilde{\varepsilon} = \bar{\varepsilon}^{p}_{i+\frac{1}{2}}/(\gamma-1).$$

Following [SM12], the inequalities (SM3.11) hold under the linear sufficient condition

$$\left(\max\left\{0, A_{i+\frac{1}{2}}\right\} + \left|B_{i+\frac{1}{2}}\right|\right)\theta_{i+\frac{1}{2}} \leqslant C_{i+\frac{1}{2}},$$

if making use of $\theta^2_{i+\frac{1}{2}} \leqslant \theta_{i+\frac{1}{2}},\ \theta_{i+\frac{1}{2}} \in [0,1]$. Thus the coefficient can be chosen as

$$\theta_{i+\frac{1}{2}} = \min\left\{1,\ \frac{C_{i+\frac{1}{2}}}{\max\{0, A_{i+\frac{1}{2}}\} + |B_{i+\frac{1}{2}}|}\right\},$$

and the final limited numerical flux is

$$\widehat{\boldsymbol{F}}^{\texttt{Lim},**}_{i+\frac{1}{2}} = \widehat{\boldsymbol{F}}^{\texttt{L}}_{i+\frac{1}{2}} + \theta_{i+\frac{1}{2}}\Delta\widehat{\boldsymbol{F}}^{\texttt{Lim},*}_{i+\frac{1}{2}}. \tag{SM3.12}$$

SM3.1.3. Shock sensor-based limiting. In 1D, the Jameson's shock sensor [SM11] is

$$(\varphi_1)_i = \frac{|\bar{p}_{i+1} - 2\bar{p}_i + \bar{p}_{i-1}|}{|\bar{p}_{i+1} + 2\bar{p}_i + \bar{p}_{i-1}|},$$

and the modified Ducros' shock sensor reduced from the 2D case [SM6] is

$$(\varphi_2)_i = \max\left\{-\frac{\bar{v}_{i+1} - \bar{v}_{i-1}}{|\bar{v}_{i+1} - \bar{v}_{i-1}| + 10^{-40}},\ 0\right\}.$$

Note that $\bar{v}_i$ and $\bar{p}_i$ are the velocity and pressure recovered from the cell average $\overline{\boldsymbol{U}}_i$. The blending coefficient is designed as

$$\theta^s_{i+\frac{1}{2}} = \exp(-\kappa(\varphi_1)_{i+\frac{1}{2}}(\varphi_2)_{i+\frac{1}{2}}) \in (0,1],$$
$$(\varphi_s)_{i+\frac{1}{2}} = \max\left\{(\varphi_s)_i, (\varphi_s)_{i+1}\right\},\ s = 1, 2,$$

where the problem-dependent parameter κ adjusts the strength of the limiting, and its optimal choice needs further investigation. The final limited numerical flux is

$$\widehat{\boldsymbol{F}}^{\texttt{Lim}}_{i+\frac{1}{2}} = \widehat{\boldsymbol{F}}^{\texttt{L}}_{i+\frac{1}{2}} + \theta^s_{i+\frac{1}{2}}\Delta\widehat{\boldsymbol{F}}^{\texttt{Lim},**}_{i+\frac{1}{2}}, \tag{SM3.13}$$

with $\Delta\widehat{\boldsymbol{F}}^{\texttt{Lim},**}_{i+\frac{1}{2}} = \widehat{\boldsymbol{F}}^{\texttt{Lim},**}_{i+\frac{1}{2}} - \widehat{\boldsymbol{F}}^{\texttt{L}}_{i+\frac{1}{2}}$, and $\widehat{\boldsymbol{F}}^{\texttt{Lim},**}_{i+\frac{1}{2}}$ given in (SM3.12).

SM3.2. Scaling limiter for point value. A first-order LLF scheme for the point value update can be written as

$$\boldsymbol{U}^{\texttt{L}}_{i+\frac{1}{2}} = \boldsymbol{U}^n_{i+\frac{1}{2}} - \frac{2\Delta t^n}{\Delta x_i + \Delta x_{i+1}}\left(\widehat{\boldsymbol{F}}^{\texttt{L}}_{i+1}(\boldsymbol{U}^n_{i+\frac{1}{2}}, \boldsymbol{U}^n_{i+\frac{3}{2}}) - \widehat{\boldsymbol{F}}^{\texttt{L}}_{i}(\boldsymbol{U}^n_{i-\frac{1}{2}}, \boldsymbol{U}^n_{i+\frac{1}{2}})\right), \tag{SM3.14}$$

with the numerical flux

$$\widehat{\boldsymbol{F}}_i^{\mathtt{L}} = \widehat{\boldsymbol{F}}^{\mathrm{LLF}}(\boldsymbol{U}_{i-\frac{1}{2}}^n, \boldsymbol{U}_{i+\frac{1}{2}}^n) = \frac{1}{2}\left(\boldsymbol{F}(\boldsymbol{U}_{i-\frac{1}{2}}^n) + \boldsymbol{F}(\boldsymbol{U}_{i+\frac{1}{2}}^n)\right) - \frac{\alpha_i}{2}\left(\boldsymbol{U}_{i+\frac{1}{2}}^n - \boldsymbol{U}_{i-\frac{1}{2}}^n\right),$$
$$\alpha_i = \max\{\varrho(\boldsymbol{U}_{i-\frac{1}{2}}^n),\ \varrho(\boldsymbol{U}_{i+\frac{1}{2}}^n)\}.$$

Similarly to Lemma SM3.1, it is straightforward to obtain the following Lemma.

LEMMA SM3.2. The LLF scheme for the point value (SM3.14) is BP under the CFL condition

$$\Delta t^n \leqslant \frac{\Delta x_i + \Delta x_{i+1}}{2(\alpha_i + \alpha_{i+1})}. \tag{SM3.15}$$

The limited solution is obtained by blending the high-order AF scheme (2.5) with the forward-Euler scheme and the LLF scheme (SM3.14) as $\boldsymbol{U}_{i+\frac{1}{2}}^{\mathtt{Lim}} = \theta_{i+\frac{1}{2}}\boldsymbol{U}_{i+\frac{1}{2}}^{\mathtt{H}} + (1 - \theta_{i+\frac{1}{2}})\boldsymbol{U}_{i+\frac{1}{2}}^{\mathtt{L}}$, such that $\boldsymbol{U}_{i+\frac{1}{2}}^{\mathtt{Lim}} \in \mathcal{G}$.

SM3.2.1. Application to scalar conservation laws. This section enforces the MP $u_{i+\frac{1}{2}}^{\min} \leqslant u_{i+\frac{1}{2}}^{\mathtt{Lim}} \leqslant u_{i+\frac{1}{2}}^{\max}$ using the scaling limiter [SM18]. The limited solution is

$$u_{i+\frac{1}{2}}^{\mathtt{Lim}} = \theta_{i+\frac{1}{2}} u_{i+\frac{1}{2}}^{\mathtt{H}} + \left(1 - \theta_{i+\frac{1}{2}}\right) u_{i+\frac{1}{2}}^{\mathtt{L}}, \tag{SM3.16}$$

with the coefficient

$$\theta_{i+\frac{1}{2}} = \min\left\{1,\ \left|\frac{u_{i+\frac{1}{2}}^{\mathtt{L}} - u_{i+\frac{1}{2}}^{\min}}{u_{i+\frac{1}{2}}^{\mathtt{L}} - u_{i+\frac{1}{2}}^{\mathtt{H}}}\right|,\ \left|\frac{u_{i+\frac{1}{2}}^{\max} - u_{i+\frac{1}{2}}^{\mathtt{L}}}{u_{i+\frac{1}{2}}^{\mathtt{H}} - u_{i+\frac{1}{2}}^{\mathtt{L}}}\right|\right\}.$$

The bounds are determined by $u_{i+\frac{1}{2}}^{\min} = \min \mathcal{N}$, $u_{i+\frac{1}{2}}^{\max} = \max \mathcal{N}$, where the set $\mathcal{N}$ consists of all the DoFs in the domain, i.e., $\mathcal{N} = \bigcup_i \{\bar{u}_i^n, u_{i+\frac{1}{2}}^n\}$ for the global MP. One can also consider the local MP, e.g., $\mathcal{N} = \left\{u_{i-\frac{1}{2}}^n, u_{i+\frac{1}{2}}^n, u_{i+\frac{3}{2}}^n\right\}$, which at least includes all the DoFs appeared in the first-order LLF scheme (SM3.14).

SM3.2.2. Application to the compressible Euler equations. The limiting consists of two steps.

i) Positivity of density. First, the high-order solution $\boldsymbol{U}_{i+\frac{1}{2}}^{\mathtt{H}}$ is modified as $\boldsymbol{U}_{i+\frac{1}{2}}^{\mathtt{Lim},*}$, such that $\boldsymbol{U}_{i+\frac{1}{2}}^{\mathtt{Lim},*,\rho} \geqslant \varepsilon_{i+\frac{1}{2}}^{\rho} := \min\{10^{-13}, \varepsilon^{\rho}, \boldsymbol{U}_{i+\frac{1}{2}}^{\mathtt{L},\rho}\}$ with ε^{ρ} given in (SM3.10). Solving the inequality yields

$$\theta_{i+\frac{1}{2}}^{*} = \begin{cases} \dfrac{\boldsymbol{U}_{i+\frac{1}{2}}^{\mathtt{L},\rho} - \varepsilon_{i+\frac{1}{2}}^{\rho}}{\boldsymbol{U}_{i+\frac{1}{2}}^{\mathtt{L},\rho} - \boldsymbol{U}_{i+\frac{1}{2}}^{\mathtt{H},\rho}}, & \text{if } \boldsymbol{U}_{i+\frac{1}{2}}^{\mathtt{H},\rho} < \varepsilon_{i+\frac{1}{2}}^{\rho}, \\ 1, & \text{otherwise.} \end{cases}$$

Then the density component of the limited solution is $\boldsymbol{U}_{i+\frac{1}{2}}^{\mathtt{Lim},*,\rho} = \theta_{i+\frac{1}{2}}^{*}\boldsymbol{U}_{i+\frac{1}{2}}^{\mathtt{H},\rho} + (1 - \theta_{i+\frac{1}{2}}^{*})\boldsymbol{U}_{i+\frac{1}{2}}^{\mathtt{L},\rho}$, with the other components remaining the same as $\boldsymbol{U}_{i+\frac{1}{2}}^{\mathtt{H}}$.

ii) Positivity of pressure. Then the limited solution $\boldsymbol{U}_{i+\frac{1}{2}}^{\mathtt{Lim},*}$ is modified as $\boldsymbol{U}_{i+\frac{1}{2}}^{\mathtt{Lim}}$, such that it gives positive pressure, i.e., $p(\boldsymbol{U}_{i+\frac{1}{2}}^{\mathtt{Lim}}) \geqslant \varepsilon_{i+\frac{1}{2}}^{p} := \min\{10^{-13}, \varepsilon^{p}, p(\boldsymbol{U}_{i+\frac{1}{2}}^{\mathtt{L}})\}$, with ε^{p} given in (SM3.10). Let the final limited solution be

$$\boldsymbol{U}_{i+\frac{1}{2}}^{\mathtt{Lim}} = \theta_{i+\frac{1}{2}}^{**}\boldsymbol{U}_{i+\frac{1}{2}}^{\mathtt{Lim},*} + \left(1 - \theta_{i+\frac{1}{2}}^{**}\right)\boldsymbol{U}_{i+\frac{1}{2}}^{\mathtt{L}}. \tag{SM3.17}$$

The pressure is a concave function of the conservative variables (see e.g. [SM20]), so that $p(\boldsymbol{U}^{\mathtt{Lim}}_{i+\frac12}) \geqslant \theta^{**}_{i+\frac12} p(\boldsymbol{U}^{\mathtt{Lim},*}_{i+\frac12}) + \left(1-\theta^{**}_{i+\frac12}\right) p(\boldsymbol{U}^{\mathrm{L}}_{i+\frac12})$ based on Jensen's inequality and $\boldsymbol{U}^{\mathtt{Lim},*,\rho}_{i+\frac12} > 0$, $\boldsymbol{U}^{\mathrm{L},\rho}_{i+\frac12} > 0$, $\theta^{**}_{i+\frac12} \in [0,1]$. Thus the coefficient can be chosen as

$$\theta^{**}_{i+\frac12} = \begin{cases} \dfrac{p(\boldsymbol{U}^{\mathrm{L}}_{i+\frac12}) - \varepsilon^{p}_{i+\frac12}}{p(\boldsymbol{U}^{\mathrm{L}}_{i+\frac12}) - p(\boldsymbol{U}^{\mathtt{Lim},*}_{i+\frac12})}, & \text{if } p(\boldsymbol{U}^{\mathtt{Lim},*}_{i+\frac12}) < \varepsilon^{p}_{i+\frac12}, \\ 1, & \text{otherwise.} \end{cases}$$

THEOREM SM3.3. If the initial numerical solution $\overline{\boldsymbol{U}}^{0}_{i}, \boldsymbol{U}^{0}_{i+\frac12} \in \mathcal{G}$ for all i, and the time step size satisfies (SM3.5) and (SM3.15), then the AF methods (2.4)-(2.5) equipped with the SSP-RK3 (2.14) and the BP limitings

- (SM3.9) and (SM3.16) preserve the maximum principle for scalar case;
- (SM3.12) and (SM3.17) preserve positive density and pressure for the Euler equations.

Remark SM3.4. For uniform meshes, and if taking the maximal spectral radius of $\partial \boldsymbol{F}/\partial \boldsymbol{U}$ in the domain as $\|\varrho\|_\infty$, the following CFL condition

$$\Delta t^n \leqslant \frac{\Delta x}{2\,\|\varrho\|_\infty}$$

fulfills the time step size constraints (SM3.5) and (SM3.15).

SM4. Additional numerical results.

Example SM4.1 (1D accuracy test for the Euler equations). This test is used to examine the accuracy of using different point value updates, following the setup in [SM1]. The domain is $[-1,1]$ with periodic boundary conditions. The adiabatic index is chosen as $\gamma = 3$ so that the characteristic equations of two Riemann invariants $w = u \pm a$ are $w_t + w w_x = 0$. The initial condition is $\rho_0(x) = 1 + \zeta \sin(\pi x), v_0 = 0, p_0 = \rho_0^{\gamma}$ and $\zeta \in (0,1)$ controls the range of the density. The exact solution can be obtained by the method of characteristics, given by $\rho(x,t) = \frac12 (\rho_0(x_1) + \rho_0(x_2)), v(x,t) = \sqrt{3}\,(\rho(x,t) - \rho_0(x_1))$, where x_1 and x_2 are solved from the nonlinear equations $x + \sqrt{3}\rho_0(x_1)t - x_1 = 0$, $x - \sqrt{3}\rho_0(x_2)t - x_2 = 0$. The problem is solved until $T = 0.1$ with $\zeta = 1 - 10^{-7}$.

As $\zeta = 1 - 10^{-7}$, the minimum density and pressure are 10^{-7} and 10^{-21} respectively, so that the BP limitings are necessary to run this test case. The maximal CFL numbers allowing stable simulations are obtained experimentally, which are around $0.47, 0.43, 0.32, 0.18$ for the JS, LLF, SW, and VH FVS, respectively, thus we run the test with the same CFL number as 0.18. Figure SM1 shows the errors and corresponding convergence rates for the conservative variables in the ℓ^1 norm. It is seen that the JS and all the FVS except for the SW FVS achieve the designed third-order accuracy, showing that our BP limitings do not affect the high-order accuracy. To examine the reason why the scheme based on the SW FVS is only second-order accurate, Figure SM2 plots the density and velocity profiles obtained using the SW FVS with 80 cells. One can observe some defects in the density when the velocity is zero, similar to the "sonic point glitch" in the literature [SM16]. One possible reason is that the SW FVS is based on the absolute value of the eigenvalues, and the corresponding mass flux is not differentiable when the velocity is zero [SM17]. Such an issue remains to be further explored in the future.

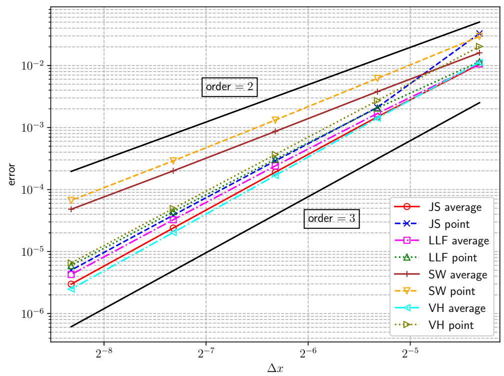

Fig. SM1: Example SM4.1, the accuracy test for the 1D Euler equations. The BP limitings are necessary.

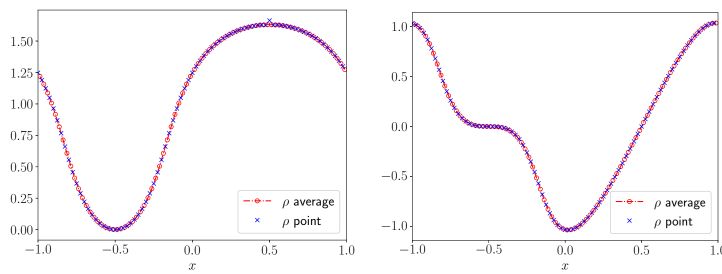

Fig. SM2: Example SM4.1, the density (left) and velocity (right) obtained with the SW FVS and 80 cells for the 1D Euler equations.

Example SM4.2 (Double rarefaction problem). The exact solution to this problem contains a vacuum, so that it is often used to verify the BP property of numerical methods. The test is solved on a domain $[0,1]$ until $T = 0.3$ with the initial data

$$(\rho, v, p) = \begin{cases} (7, -1, 0.2), & \text{if} \quad x < 0.5, \\ (7, 1, 0.2), & \text{otherwise}. \end{cases}$$

In this test, the AF method based on any kind of point value update mentioned in this paper gives negative density or pressure without the BP limitings. Figure SM3 shows the density computed with 400 cells and the BP limitings for the cell average and point value updates. The CFL number is 0.4 for all kinds of point value updates, except for 0.1 for the VH FVS. One observes that the BP AF method gets good performance for this example.

Example SM4.3 (Blast wave interaction). The power law reconstruction is useful to reduce oscillations for the fully-discrete AF method [SM3], thus we would also like to test its ability for the generalized (semi-discrete) AF method. Figure SM4 shows the density profiles and corresponding enlarged views obtained by using the BP limitings and power law reconstruction on a uniform mesh of 800 cells. It is seen that the power law reconstruction can suppress oscillations, but the results are still more oscillatory than those using the shock sensor-based limiting. Note that the CFL number reduces

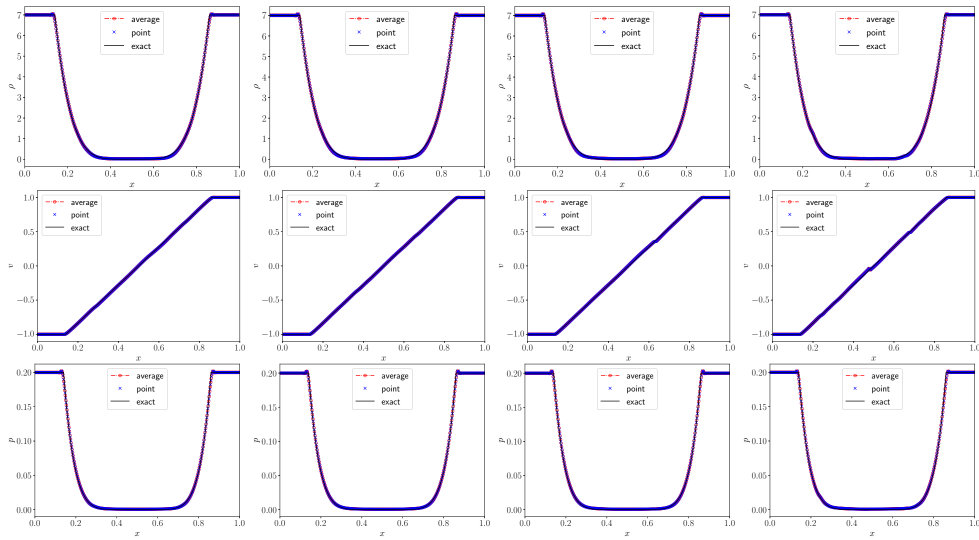

Fig. SM3: Example SM4.2, double rarefaction Riemann problem. The density, velocity, and pressure are computed by the BP AF methods on a uniform mesh of 400 cells. From left to right: JS, LLF, SW, and VH FVS.

to 0.1 when the power law reconstruction is activated. This kind of reduction of the CFL number is also observed in other test cases thus we do not recommend using the power law reconstruction for the generalized AF methods, which also motivates us to develop the shock sensor-based limiting.

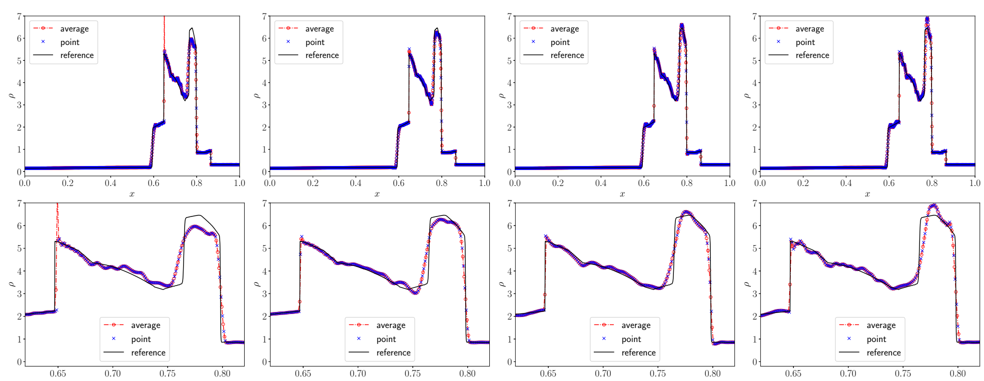

Fig. SM4: Example 5.3, blast wave interaction. The density computed with the power law reconstruction and BP limitings, and the corresponding enlarged views in $[0.62, 0.82]$ are shown in the bottom row. From left to right: JS, LLF, SW, and VH FVS.

Example SM4.4 (Double Mach reflection). The computational domain is $[0,3] \times [0,1]$ with a reflective wall at the bottom starting from $x = 1/6$. A Mach 10 shock is moving towards the bottom wall with an angle of $\pi/6$. The pre- and post-shock states are

$$(\rho, v_1, v_2, p) = \begin{cases} (1.4,\ 0,\ 0,\ 1), & x \geqslant 1/6 + (y + 20t)/\sqrt{3}, \\ (8,\ 8.25\cos(\pi/6), -8.25\sin(\pi/6),\ 116.5), & x < 1/6 + (y + 20t)/\sqrt{3}. \end{cases}$$

The reflective boundary condition is applied at the wall, while the exact post-shock condition is imposed at the left boundary and for the rest of the bottom boundary (from $x = 0$ to $x = 1/6$). At the top boundary, the exact motion of the Mach 10 shock is applied and the outflow boundary condition is used at the right boundary. The results are shown at $T = 0.2$.

The AF method without the BP limitings gives negative density or pressure near the reflective location $(1/6, 0)$, so the BP limitings are necessary for this test. The numerical solutions are computed without or with the shock sensor ($\kappa = 1$) on a series of uniform meshes. The density plots with enlarged views around the double Mach region are shown in Figure SM5, and the blending coefficients based on the shock sensor are shown in Figure SM6. When the shock sensor is not activated, the noise after the bow shock is obvious, and it is damped with the help of the shock sensor. As mesh refinement, the numerical solutions converge with a good resolution and are comparable to those in the literature. Compared to the third-order P^2 DG method using the TVB limiter [SM4] with the same mesh resolution ($\Delta x = \Delta y = 1/480$), the roll-ups and vortices are comparable while the AF method uses fewer DoFs (4 versus 6 per cell).

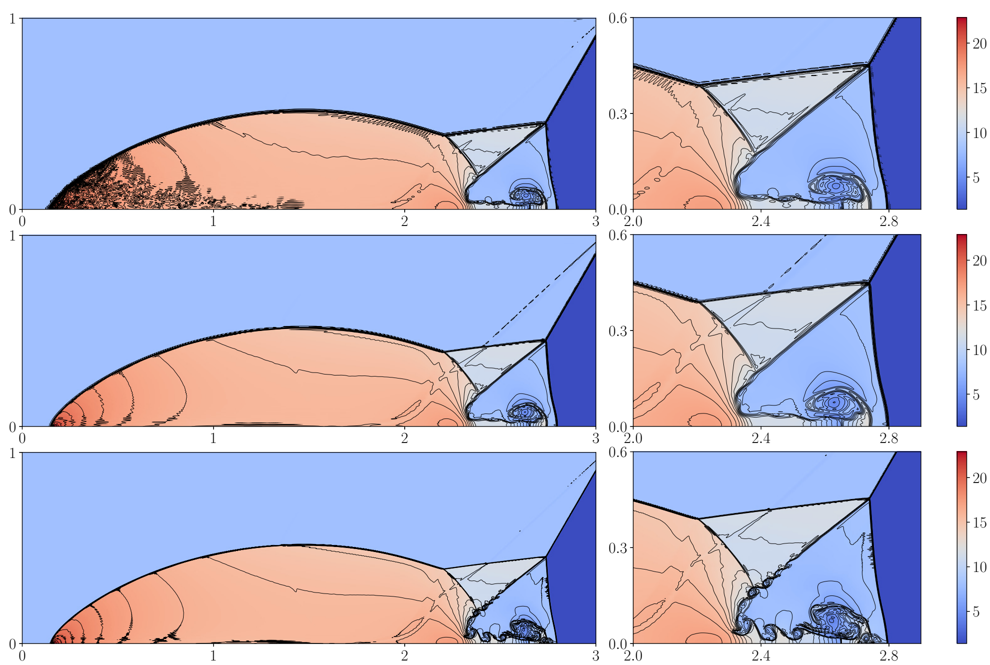

Fig. SM5: Example SM4.4, double Mach reflection. The density obtained with the BP limitings and without or with the shock sensor. From top to bottom: 720×240 mesh without shock sensor, 720×240 mesh with $\kappa = 1$, 1440×480 mesh with $\kappa = 1$. 30 equally spaced contour lines from 1.390 to 22.861.

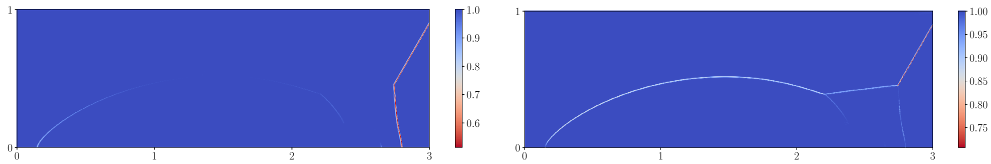

Fig. SM6: Example SM4.4, double Mach reflection. The blending coefficients $\theta^s_{i+\frac{1}{2},j}$ (left) and $\theta^s_{i,j+\frac{1}{2}}$ (right) based on the shock sensor with $\kappa = 1$ on the 1440×480 mesh.

REFERENCES

[SM1] R. Abgrall, *A combination of residual distribution and the active flux formulations or a new class of schemes that can combine several writings of the same hyperbolic problem: Application to the 1D Euler equationss*, Commun. Appl. Math. Comput., 5 (2023), pp. 370–402, https://doi.org/10.1007/s42967-021-00175-w.

[SM2] R. Abgrall, J. Lin, and Y. Liu, *Active flux for triangular meshes for compressible flows problems*, Dec. 2023, https://doi.org/10.48550/arxiv.2312.11271, https://arxiv.org/abs/2312.11271.

[SM3] W. Barsukow, *The active flux scheme for nonlinear problems*, J. Sci. Comput., 86 (2021), p. 3, https://doi.org/10.1007/s10915-020-01381-z.

[SM4] B. Cockburn and C. W. Shu, *Runge-Kutta discontinuous Galerkin methods for convection-dominated problems*, J. Sci. Comput., 16 (2001), pp. 173–261, https://doi.org/10.1023/a:1012873910884.

[SM5] C. M. Dafermos, *Hyperbolic Conservation Laws in Continuum Physics*, Springer Berlin Heidelberg, 2000, https://doi.org/10.1007/978-3-662-22019-1.

[SM6] F. Ducros, V. Ferrand, F. Nicoud, C. Weber, D. Darracq, C. Gacherieu, and T. Poinsot, *Large-eddy simulation of the shock/turbulence interaction*, Journal of Computational Physics, 152 (1999), pp. 517–549, https://doi.org/10.1006/jcph.1999.6238, https://www.sciencedirect.com/science/article/pii/S0021999199962381 (accessed 2024-05-29).

[SM7] J.-L. Guermond, M. Nazarov, B. Popov, and I. Tomas, *Second-order invariant domain preserving approximation of the Euler equations using convex limiting*, SIAM J. Sci. Comput., 40 (2018), pp. A3211–A3239, https://doi.org/10.1137/17M1149961.

[SM8] J.-L. Guermond and B. Popov, *Invariant domains and first-order continuous finite element approximation for hyperbolic systems*, SIAM J. Numer. Anal., 54 (2016), pp. 2466–2489, https://doi.org/10.1137/16M1074291.

[SM9] J.-L. Guermond, B. Popov, and I. Tomas, *Invariant domain preserving discretization-independent schemes and convex limiting for hyperbolic systems*, Comput. Method. Appl. M., 347 (2019), pp. 143–175, https://doi.org/10.1016/j.cma.2018.11.036, https://www.sciencedirect.com/science/article/pii/S0045782518305954 (accessed 2024-03-12).

[SM10] H. Hajduk, *Monolithic convex limiting in discontinuous Galerkin discretizations of hyperbolic conservation laws*, Comput. Math. Appl., 87 (2021), pp. 120–138, https://doi.org/10.1016/j.camwa.2021.02.012, https://www.sciencedirect.com/science/article/pii/S0898122121000547 (accessed 2024-03-12).

[SM11] A. Jameson, W. Schmidt, and E. Turkel, *Solutions of the Euler equations by finite volume methods using Runge-Kutta time-stepping schemes*, AIAA J., 1259 (1981).

[SM12] D. Kuzmin, *Monolithic convex limiting for continuous finite element discretizations of hyperbolic conservation laws*, Computer Methods in Applied Mechanics and Engineering, 361 (2020), p. 112804, https://doi.org/10.1016/j.cma.2019.112804, https://www.sciencedirect.com/science/article/pii/S0045782519306966 (accessed 2024-03-12).

[SM13] D. Kuzmin, R. Löhner, and S. Turek, eds., *Flux-Corrected Transport: Principles, Algorithms, and Applications*, Scientific Computation, Springer Netherlands, Dordrecht, 2012, https://doi.org/10.1007/978-94-007-4038-9.

[SM14] X.-D. Liu and S. Osher, *Nonoscillatory high order accurate self-similar maximum principle satisfying shock capturing schemes I*, SIAM J. Numer. Anal., 33 (1996), pp. 760–779, https://doi.org/10.1137/0733038.

[SM15] B. Perthame and C.-W. Shu, *On positivity preserving finite volume schemes for Euler equations*, Numer. Math., 73 (1996), pp. 119–130, https://doi.org/10.1007/s002110050187.

[SM16] H. Z. Tang, *On the sonic point glitch*, J. Comput. Phys., 202 (2005), pp. 507–532, https://doi.org/10.1016/j.jcp.2004.07.013, https://www.sciencedirect.com/science/article/pii/S0021999104002967 (accessed 2024-03-21).
[SM17] B. van Leer, *Flux-vector splitting for the Euler equations*, in Eighth International Conference on Numerical Methods in Fluid Dynamics, E. Krause, ed., Lecture Notes in Physics, Berlin, Heidelberg, 1982, Springer, pp. 507–512, https://doi.org/10.1007/3-540-11948-5_66.
[SM18] X. Zhang and C.-W. Shu, *On maximum-principle-satisfying high order schemes for scalar conservation laws*, J. Comput. Phys., 229 (2010), pp. 3091–3120, https://doi.org/10.1016/j.jcp.2009.12.030, https://www.sciencedirect.com/science/article/pii/S0021999109007165 (accessed 2024-06-14).
[SM19] X. Zhang and C.-W. Shu, *On positivity-preserving high order discontinuous Galerkin schemes for compressible Euler equations on rectangular meshes*, J. Comput. Phys., 229 (2010), pp. 8918–8934, https://doi.org/10.1016/j.jcp.2010.08.016, https://www.sciencedirect.com/science/article/pii/S0021999110004535 (accessed 2024-03-26).
[SM20] X. Zhang and C.-W. Shu, *Maximum-principle-satisfying and positivity-preserving high-order schemes for conservation laws: survey and new developments*, Proceedings of the Royal Society A: Mathematical, Physical and Engineering Sciences, 467 (2011), pp. 2752–2776, https://doi.org/10.1098/rspa.2011.0153.
[SM21] X. Zhang and C.-W. Shu, *Positivity-preserving high order discontinuous Galerkin schemes for compressible Euler equations with source terms*, J. Comput. Phys., 230 (2011), pp. 1238–1248, https://doi.org/10.1016/j.jcp.2010.10.036, https://www.sciencedirect.com/science/article/pii/S0021999110006017 (accessed 2024-03-13).